# Enhanced Thermoelectric Performance of Holey Silicon Thin Films using F<sub>4</sub>TCNQ Surface Doping

Tianhui Zhu<sup>a,1</sup>, Yunhui Wu<sup>b,1</sup>, Shuai Li<sup>c</sup>, Farjana F. Tonni<sup>a</sup>, Masahiro Nomura<sup>b</sup>, Mona Zebarjadi<sup>a,c</sup>,

<sup>a</sup>Department of Electrical and Computer Engineering, University of
Virginia, Charlottesville, 22904, VA, USA

<sup>b</sup>Institute of Industrial Science, The University of Tokyo, Tokyo, 153-8505, Japan

<sup>c</sup>Department of Materials Science and Engineering, University of Virginia,
Charlottesville, 22904, VA, USA

#### Abstract

Silicon thin films have great potential as chip-integrated Peltier micro-coolers and thermoelectric power generators due to their industry compatibility and cost effectiveness. Improving the thermoelectric figure of merit, zT, and therefore the device efficiency can be achieved by increasing the power factor while decreasing the thermal conductivity. In this work, we study single crystalline silicon thin films with patterned nano-holes with sizes comparable to the phonon mean free path to suppress thermal conductivity. The holey silicon thin films are then surface doped with organic molecules F<sub>4</sub>TCNQ to create a threedimensional modulation doping scheme. As the dopants are outside the host material, there is less impurity scattering, which improves carrier mobility and the overall power factor. We fabricate silicon thin films with periodic arrays of nano-sized holes, with a fixed pitch size of 300nm. By changing the hole diameters, we vary the neck size from 169nm to 22nm. The in-plane thermal conductivity, measured using the heat diffusion imaging method, demonstrates an order of magnitude reduction compared to bulk silicon and a change from 26Wm<sup>-1</sup>K<sup>-1</sup> to 5Wm<sup>-1</sup>K<sup>-1</sup> at room temperature. The films with large hole diameters allow space for the relatively large F4TCNQ molecules and hence effective surface doping, which is evident by orders of magnitude improvement in the electrical conductivity and power factor.

Email addresses: nomura@iis.u-tokyo.ac.jp (Masahiro Nomura ), m.zebarjadi@virginia.edu (Mona Zebarjadi )

<sup>&</sup>lt;sup>1</sup>T.Z. and Y.W. contributed equally to this work.

## 1. Introduction

Silicon thin films are potential candidates for thermoelectric applications such as on-chip thermal management [1] and power generation for wearable electronics [2], due to their industrial process compatibility and cost-effectiveness. It is shown that silicon thin-films are flexible and upon transfer to flexible substrates, they can be used for wearable electronic applications [3, 4]. The efficiency of thermoelectric power generators and the coefficient of performance of Peltier coolers are an increasing function of the thermoelectric figure of merit,  $zT = \sigma S^2 T/\kappa$ , where  $\sigma$  is the electrical conductivity, S is the Seebeck coefficient and  $\kappa$  is the thermal conductivity. Improving the zT of a material can be achieved by increasing the power factor ( $PF = \sigma S^2$ ) while decreasing the thermal conductivity  $\kappa$ .

An effective route to reducing the thermal conductivity of Si is through the addition of nanostructures [5, 6] or increasing surface roughness [7], which induces more frequent phonon scattering and limits the phonon mean free path (MFP). This has been implemented on Si thin films, by patterning arrays of nanosized holes [8, 9, 10, 11, 12, 13]. These silicon thin films with an array of holes are referred to as holey Si thin films or sometimes as phononic crystals. Research has shown that the thermal conductivity depends on the neck size, i.e., the distance between adjacent holes [5, 6]. The reduction in thermal conductivity can be one or almost two orders of magnitude compared to thin film without holes, depending on the neck size and the temperature [10, 14]. In these structures, an optimum design is to have neck sizes in between the electron and the phonon MFP to selectively limit phonon diffusion with minimum effect on electron mobility, enabling *zT* improvement [10, 11, 12, 13].

Most thermoelectric materials are made out of heavily doped semiconductors. Bulk silicon demonstrates the maximum thermoelectric power factor at high doping levels (around  $10^{20}$  cm<sup>-3</sup>) [15]. Conventional doping techniques insert dopant atoms into the host materials. These dopants introduce strong Coulomb repulsion and reduce carrier mobility. In comparison, surface charge transfer doping is a clean and effective alternative, where charges exchange across the interface between the surface dopants and the host material due to energy band misalignment [16]. The ionized atoms are therefore distanced from the mobile charge carriers and a space-charge layer is formed at

the interface. As the dopants are outside the host material, the extra space between the dopants and the carriers lowers the ionized impurity interactions significantly. This is similar to the modulation doping idea used in transistors. The electron mobility in GaAs, for instance, has been enhanced by 4 orders of magnitudes using modulation doping strategy at below 10K [17].

The organic molecule,  $F_4TCNQ$  (2,3,5,6-tetrafluoro-7,7,8,8-tetracyanoquinodimethane), is a strong electron acceptor with an electron affinity as high as  $E_a$  = 5.24eV [18] and is often used as a p-type surface dopant for organic [19, 20] and inorganic [21, 22, 23] materials. First-principles calculations predict that physisorbed  $F_4TCNQ$  monolayer can efficiently dope Si [24], achieving a surface hole concentration as high as  $10^{13}$  cm<sup>-2</sup>. An experimental study on the transport properties at  $F_4TCNQ$ -Si interface demonstrated a resistance reduction by a factor of 10 compared to undoped film and a thermoelectric *PF* enhancement by 75% [25].

In this work, we extend the surface doping to three dimensions (3D). In a 2D geometry, while the thermoelectric power factor can be extremely large [26], one has to deal with an electron gas with a large thermal conductivity. The modulation doping concept has been extended to 3D in the past and improved zT has been shown in SiGe nanostructures [27, 28]. The improvement, in that case, was limited due to the grain-boundary scattering. Here, we propose the usage of holey silicon thin films to demonstrate 3D surface doping in organic-inorganic structures. The holey silicon films are clean with minimal scattering due to the periodic nature of holes and clean thin-film fabrication process, compared to the nanostructured bulk samples [27, 28] with irregular grain boundaries and impurities. They provide a possible geometry for a 3D network of organic dopants and effective doping not only from the top surface but also from within the film.

We fabricate single crystalline Si thin films with square lattice arrays of nanosized holes of different diameters and surface-dope them with  $F_4TCNQ$ . We report improvement in electrical conductivity by a factor as high as 350 and in the thermoelectric power factor by a factor as high as 200 after the deposition of  $F_4TCNQ$ , demonstrating the effectiveness of 3D surface doping. This is combined with the low thermal conductivity of the silicon films due to the presence of the holes to enhance the zT by 2 orders of magnitudes.

#### Material and Methods

The holey silicon thin-film devices were fabricated from silicon-on-insulator

(SOI) wafers, which had an active Si layer of 220nm thickness on top of a  $3\mu$ m-thick SiO<sub>2</sub> layer. We used laser lithography and reactive ion etching (RIE) to

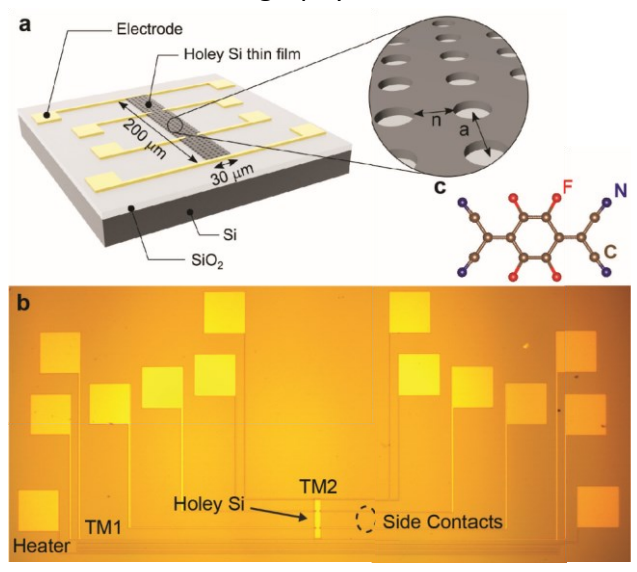


Figure 1: (a) Schematic and (b) optical image of the holey silicon device, which includes one heater, two thermometers (TMs) and four side contacts. The scale bar is 500  $\mu$ m. (c) Molecular structure of F<sub>4</sub>TCNQ.

define device areas of  $200\times30~\mu\text{m}^2$ . Subsequently, e-beam lithography and RIE patterned the nano-sized hole arrays onto each device. The holes were kept at a fixed pitch distance of a=300nm, and the neck size n of each device varied from 22nm to 169nm. Limited by the capability of the e-beam lithography tool, the smallest neck size we could reliably pattern was 22nm. Lastly, electrodes (500nm Al and 50nm Au) were evaporated onto the sample to serve as thermometers, heaters, and voltage probes. The Si layer was mildly boron-doped with a resistivity of  $10\Omega\cdot\text{cm}$ , which corresponds to a hole concentration of  $\sim 10^{15}\,\text{cm}^{-3}$ . The regions under the contacts were doped to  $10^{20}\,\text{cm}^{-3}$  to ensure Ohmic contacts. Schematics of the hole configuration, as well as the device configuration, are shown in Fig.1.

 $F_4$ TCNQ crystal powder was thermally evaporated in a home-built vacuum chamber with a base pressure of  $< 10^{-6}$  Torr. The deposition temperature was maintained at about  $140\,^{\circ}$  C, following the methods described in previous work [25]. The samples were dipped in 10% HF for a few seconds right before being loaded into the evaporation chamber, in order to remove the native oxide and

passivate the Si surface. The structure of the  $F_4TCNQ$  molecule is presented in Fig.1(c), with a unit cell of  $7.5 \times 11.7 \times 5.9 \text{Å}^3$ .

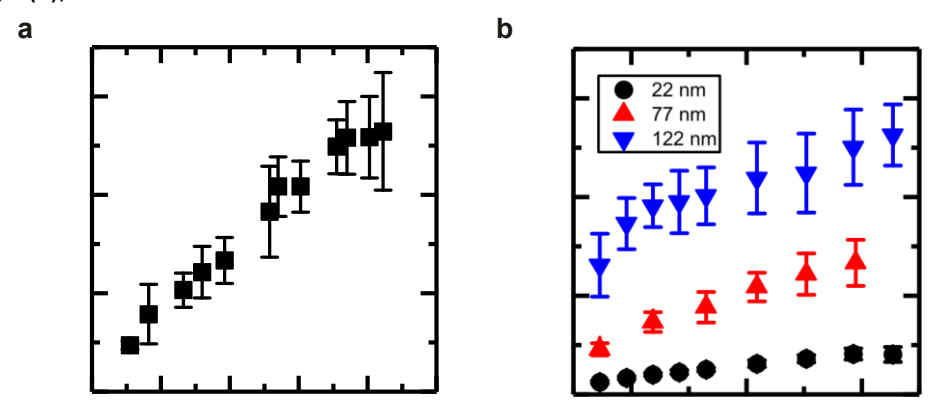


Figure 2: (a) Room temperature in-plane thermal conductivity for neck sizes from 22nm to 169nm and (b) temperature-dependent thermal conductivity from 50K to 350K for neck sizes 22nm, 77nm, and 122nm.

The electrical resistance was measured by the standard 4-point probe method and the conductivity was calculated assuming a solid thin film. The Seebeck voltage was measured by a Keithley 2182A nanovoltmeter and the temperature difference was interpreted from the resistance changes of the two gold thermistors at the two ends of the thin film.

Heat diffusion imaging [14] was used to measure the in-plane thermal conductivity. This is an electrical-pump optical-probe method that provides accurate readings for supported thin films using thermoreflectance-based techniques. A voltage pulse is passed through the thermometer placed directly on top of the thin film. As the injected heat flow propagates along the thin film of interest, a temperature map is calculated from the surface reflectivity changes. The thermal conductivity values are extracted based on how the temperature rise decays over distance. The details of the method and the process of extracting the thermal conductivity values of supported films are described in our previous work [14].

## 3. Results and Discussion

The in-plane thermal conductivity of the holey silicon thin film depends on the neck size. Figure 2 shows that as the neck size goes down from 169nm to 22nm, the room temperature thermal conductivity decreases from 26.4Wm<sup>-1</sup>K<sup>-1</sup>

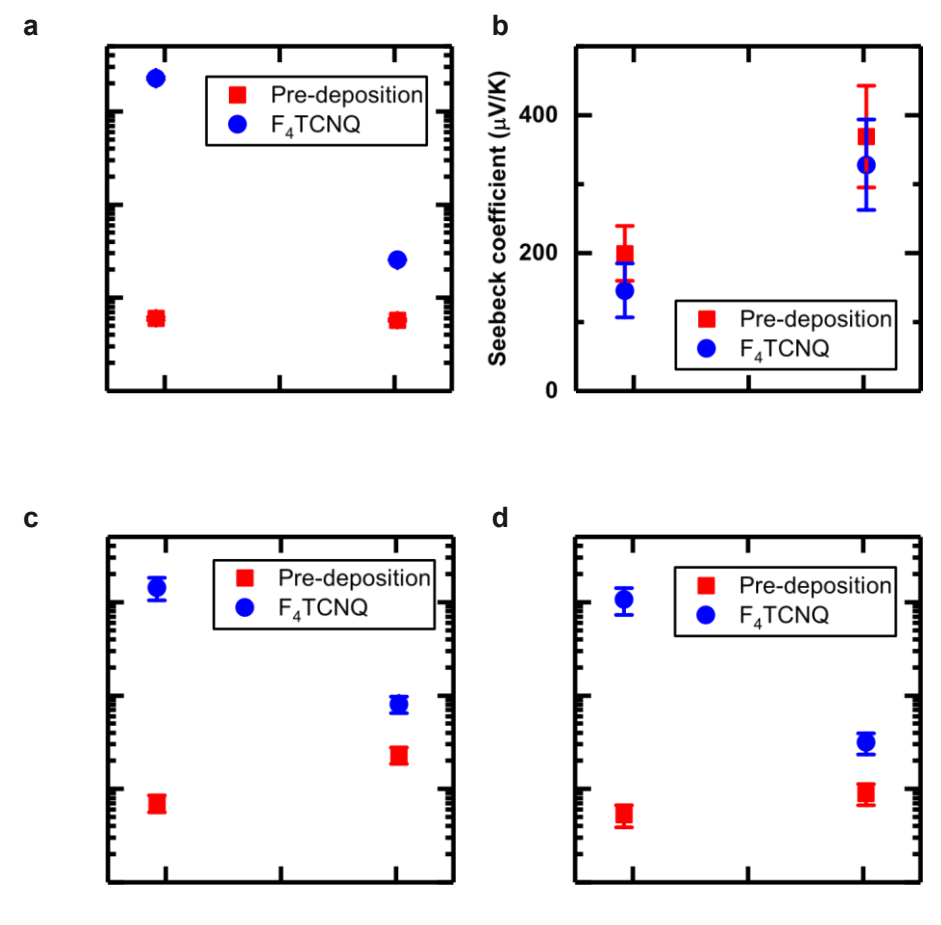


Figure 3: Comparison of the thermoelectric performance of the 77nm neck and 161nm neck devices before and after F<sub>4</sub>TCNQ deposition at room temperature, in terms of (a) electrical conductivity, (b) Seebeck coefficient, (c) PFT, and (d) zT.

to 4.7Wm<sup>-1</sup>K<sup>-1</sup>, nearly 5 times. Smaller neck size suppresses the phonon transport more and leads to smaller thermal conductivity values. The trend is consistent with those summarized in the literature [5, 6]. In comparison, the room temperature thermal conductivity of a silicon thin film of the same

thickness without any holes is about 90Wm<sup>-1</sup>K<sup>-1</sup> [29]. The reduction in thermal conductivity with periodic holes is as high as 19-fold.

The thermal conductivity of three different neck sizes as a function of temperature was also obtained and is plotted in Fig.2. Their temperature-dependent trends are consistent: as the temperature increases from 75K to above room temperature, the thermal conductivity increases, and the rate of change becomes smaller at higher temperatures. The overall change in this range is about 2 to 3 times.

The electrical transport of the thin film with neck sizes of 77nm and 161nm before and after the F<sub>4</sub>TCNQ deposition was measured at room temperature. For both samples, their electrical conductivity started at around 60S/m. With F<sub>4</sub>TCNQ, the conductivity of the 77nm sample increased by 2 orders of magnitude and reached 2.28×10<sup>4</sup> S/m, while that of the 161nm sample increased to 255S/m, slightly over 4 times higher. As expected, the Seebeck coefficients of both samples dropped after doping, by about 10-20%. As a result, the power factor times temperature (PFT) was improved by 4 times for the 161nm neck sample and by 200 times for the 77nm one. The doping by F<sub>4</sub>TCNQ here is more effective compared to the case of silicon thin film without holes[25]. A PFT as high as 0.14Wm<sup>-1</sup>K<sup>-1</sup> was achieved for the doped 77nm sample, which is on the same order of magnitude compared to highly-doped Si thin film samples from the literature [10, 30]. Unfortunately, due to electrical contact problems, we were not able to measure the neck-size dependence of the electrical conductivity and the Seebeck coefficient systematically as we did for the case of thermal conductivity. Among the prepared samples, only the 77nm and the 161nm samples had small and Ohmic contact resistances allowing electrical transport measurement.

Considering the two measured samples, several factors are deciding the effectiveness of the F<sub>4</sub>TCNQ doping. First is the orientation of the molecules. It has been shown that when the molecules lay parallel to the surface, the charge transfer is small [24]. F<sub>4</sub>TCNQ doping is only effective when the molecular long axis is normal to the silicon surface. Second, because the F<sub>4</sub>TCNQ molecules tend to form clusters during the deposition process, the holes have to be large enough for the molecules to enter properly and attach to the inner cylindrical walls effectively.

Figure 4 shows SEM images taken after 15 minutes of F<sub>4</sub>TCNQ deposition on both 77nm and 161nm samples. When the holes are small, the clusters extend over and cover the top surface of the holes. This is the case for the 161nm

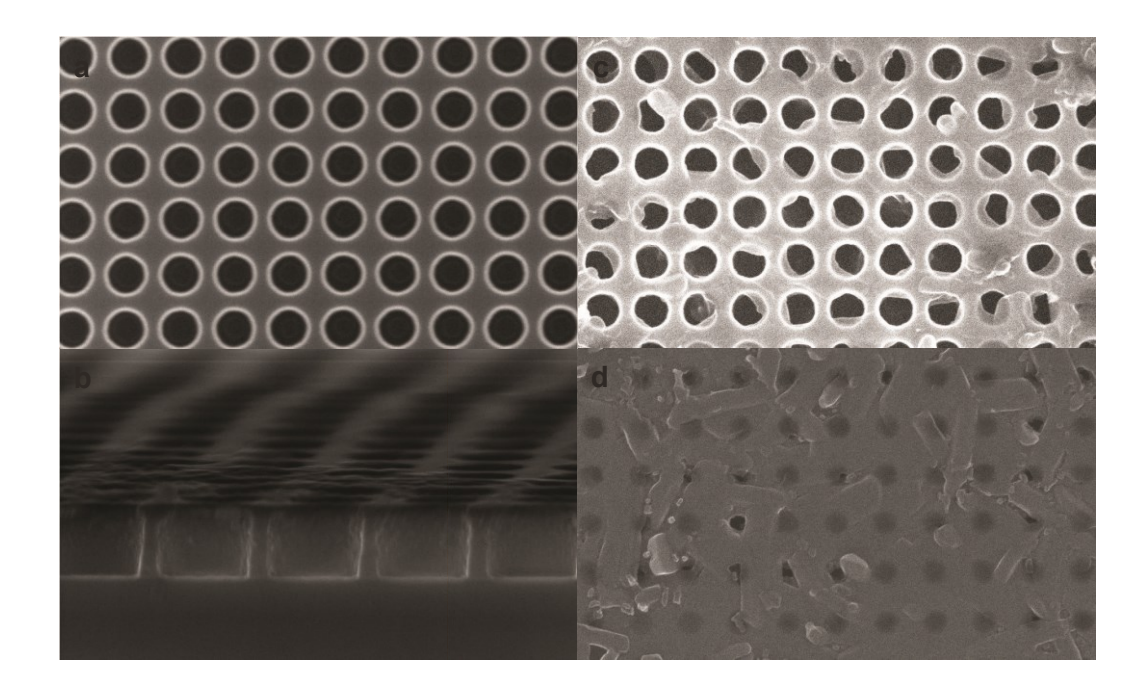


Figure 4: Scanning electron microscope (SEM) images of (a) the hole configuration for the 77nm neck size sample, (b) cross-sectional view of the holes, (c) the 77nm neck size sample after F<sub>4</sub>TCNQ deposition and (d) the 161nm neck size sample after F<sub>4</sub>TCNQ deposition. The scale bars are  $500 \, \mu \text{m}$ .

sample with smaller holes (corresponding to 139nm hole diameter) as shown in Fig.4d. We hypothesize that this full coverage occurs before the molecules enter the holes and hence it blocks the pathway to the side walls for the incoming molecules, preventing them from entering the holes. In contrast, the holes of the 77nm sample with larger holes are only covered partially as shown in Fig.4c, allowing molecules to enter the holes. More SEM images and EDS analysis are provided in the supplementary materials.

Finally, F<sub>4</sub>TCNQ has a low sticking probability on H-Si(100) [31] and limited wettability making the deposition processes only successful when high flux and long time deposition are used [25]. Considering that the 161nm neck size sample only demonstrates 4 times conductivity improvement compared to the 200 times improvement observed in the 77nm neck size sample (223nm hole diameter), we can infer that in the latter sample, more F<sub>4</sub>TCNQ molecules entered the holes and attached normal to the walls. In other words, the 77nm neck size sample has a larger overall surface coverage. However, we note that the difference in the surface area coverage is only a factor of 2.4 and is not enough to explain the large

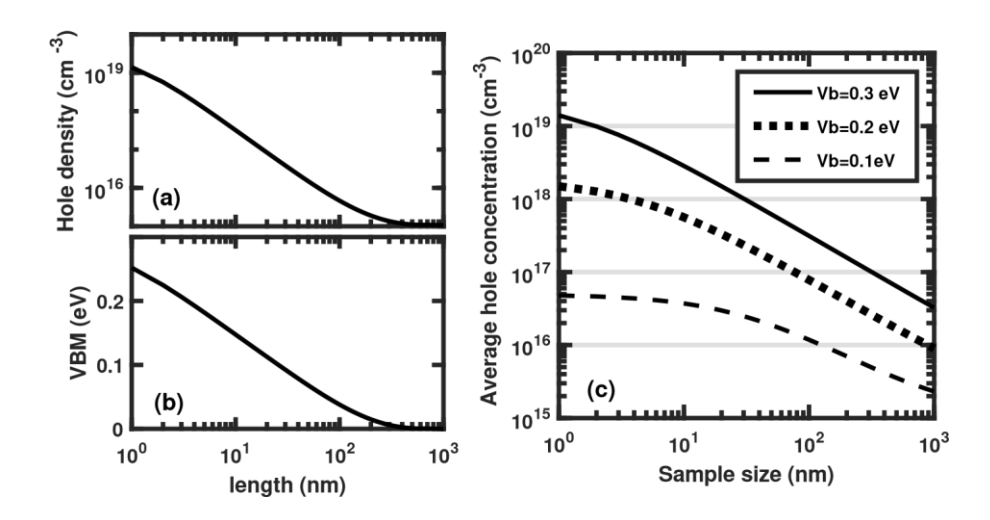


Figure 5: 1D Possion solver for charge transfer between  $F_4TCNQ$  and silicon. (a) Hole density and (b) valence band maximum as a function of the length into the silicon from the surface. (c) Average total hole concentration versus effective sample size, where  $V_b$  is the built-in potential.

### benefit here.

To explain the large difference, we have developed a 1D Poisson solver to help us better understand the doping effect at the F<sub>4</sub>TCNQ-Si interface. The model considers F<sub>4</sub>TCNQ as a metal-like source of hole carriers and calculates the charge transfer and the band bending inside the silicon structure, assuming that the Fermi level is pinned by the F<sub>4</sub>TCNQ molecules. Parameters of Si, including its effective mass (0.81 for hole and 1.81 for electron density of states effective masses respectively), bandgap (1.12eV), work function, and dielectric constant (11.7), are well-known [32]. The position of the chemical potential of silicon before F<sub>4</sub>TCNQ deposition can be calculated knowing the initial doping density of silicon (10<sup>15</sup> cm<sup>-3</sup>) and it is 0.3eV below the middle of the gap. Besides the silicon parameters, the relative alignment of the F<sub>4</sub>TCNQ energy levels to the bands of silicon determines the amount of charge transfer.

Wang et al.[24] calculated the charge transfer energy of a single  $F_4TCNQ$  molecule on a silicon surface using first-principles calculations. They reported that the difference between the electron affinity of the  $F_4TCNQ$  molecule and the valence band maxima of silicon is about -0.01eV and 0.17eV using PBE and GW calculations respectively. We also note that the levels are modified when studying a single molecule compared to bulk. The electron affinity of  $F_4TCNQ$  is reported to be between 5.08-5.24eV[33] and the work function of Si(100) is

reported to be around 4.91 eV[34]. The difference results in a built-in potential,  $V_b$ , between 0.1 to 0.3 eV at the silicon- $F_4$ TCNQ interface, so we have solved for  $V_b = 0.1,0.2,0.3$  eV using our Poisson model. Charge transfer occurs primarily at the surface and drops rapidly perpendicular to the surface. Hence, we expect a strong size dependence. Figure5a and b show the charge carrier density and the potential profile (valence band maximum) along a 1D sample respectively. As expected, the doping effect is the strongest at the interface and gradually decreases as we move deeper into the sample. The hole concentration starts from  $10^{19}$  cm<sup>-3</sup> at the interface (zero length represents the interface of  $F_4$ TCNQ and silicon) and slowly drops to the initial doping level of  $10^{15}$  cm<sup>-3</sup> after over 300nm in length. Figure5c shows the effect of Fermi level pinning. As the Fermi level is pinned deeper in the valence band, the built-in potential is larger and the charge transfer is also larger.

Let us now map this 1D model onto the 3D geometry. Assuming that in the 161nm neck size (139nm hole diameter) case the dopants either did not enter the holes or if they did, they did not effectively align inside, then only the top surface is doped. The effective size of the sample is the thickness of the film, 220nm. Figure 5c shows that for a size of 220 nm, the carrier concentration can be improved to between  $5\times10^{15}$  to  $1.1\times10^{17}$  cm<sup>-3</sup> depending on the built-in potential. In the 77nm neck size (223nm hole diameter) case, and assuming effective doping from the inner walls, the size is now half of the neck size, 39nm. At this length, the carrier concentration improves to between  $2\times10^{16}$  to  $7.9\times10^{17}$  cm<sup>-3</sup>, corresponding to a 20 to 800 times improvement of the conductivity after F<sub>4</sub>TCNQ deposition. The overlap of the charges from the top and side surfaces can further increase these numbers.

We conclude that small neck sizes correspond to significantly larger carrier concentrations and enhanced power factors after doping. A smaller neck size also means smaller thermal conductivity, which is advantageous for better zT. In the current study, zT of the 77nm sample reached 0.01 after F<sub>4</sub>TCNQ doping, demonstrating 2 orders of magnitude improvement. We, therefore, believe that even smaller neck sizes can further improve the zT.

Here we compare the obtained zT with conventionally doped samples at room temperature. zT of 0.01 in this work is one order of magnitude smaller than that of highly-doped nanocrystalline bulk Si samples  $(4\times10^{20} \, \text{cm}^{-3})$  [35] but is comparable to highly-doped single crystal bulk Si  $(10^{20} \, \text{cm}^{-3})$  [15] and higher than single crystal with mid-level doping  $(10^{18} - 10^{19} \, \text{cm}^{-3})$  [15, 36]. While our zT is lower than some highly-doped holey Si thin films with smaller thicknesses and smaller neck sizes[10, 12], it is comparable to others[11]. This shows that surface

charge transfer doping via F<sub>4</sub>TCNQ deposition is an effective approach to introduce additional charge carriers into Si thin films. The improvement in the thermoelectric performance of holey Si thin films can be further optimized by considering factors including film thickness, neck sizes and surface dopants.

## 4. Conclusion

In conclusion, we fabricated Si thin films with periodic nm-sized holes from SOI wafers and performed surface charge transfer doping with F<sub>4</sub>TCNQ organic molecules. The in-plane thermal conductivity depends on the neck size and changed from 26Wm<sup>-1</sup>K<sup>-1</sup> to 5Wm<sup>-1</sup>K<sup>-1</sup> as the neck size decreased from 169nm to 22nm. The F<sub>4</sub>TCNQ molecules were deposited via thermal evaporation. The sample with a larger hole diameter allowed more space for the F<sub>4</sub>TCNQ molecules and the surface doping was more effective. *PF* and *zT* of the 77nm neck sample improved by 2 orders of magnitude. The large improvement was possible because the holey structure extended the surface doping effect to 3D. This study demonstrates the possibility of building high-performance thermoelectric devices out of an organic-holey Si hybrid structure. Further evaluation of the holey Si geometry, the dopant materials and the manipulation of dopant molecule orientation is expected to bring even more enhancement in the thermoelectric properties. Systems with larger surface-to-volume ratios, such as nanowires, should also benefit from this doping scheme.

## Acknowledgments

We acknowledge the support of NSF grant number 1653268 and CREST JST grant Number JPMJCR19Q3. The authors thank Ryoto Yanagisawa and Junichiro Shiomi for the discussions on sample fabrication.

# Data Availability

The data that support the findings of this study are available from the corresponding authors upon reasonable request.

References

[1] G. Snyder, M. Soto, R. Alley, D. Koester, B. Conner, Hot spot cooling using embedded thermoelectric coolers, in: Twenty-Second Annual IEEE Semiconductor Thermal Measurement And Management Symposium, IEEE, 2006, pp. 135–143. doi:10.1109/STHERM.2006.1625219.

URL http://ieeexplore.ieee.org/document/1625219/

[2] V. Leonov, R. Vullers, Wearable Thermoelectric Generators for BodyPowered Devices, Journal of Electronic Materials 38 (7) (2009) 1491– 1498.

doi:10.1007/s11664-008-0638-6.

URL http://link.springer.com/10.1007/s11664-008-0638-6

- [3] S. Park, Y. H. Lee, J.-S. Wi, J. Oh, A semitransparent and flexible single crystal si thin film: Silicon on nothing (son) revisited, ACS Applied Materials Interfaces 8 (29) (2016) 18962–18968. doi:10.1021/acsami.6b05261. URL https://pubs.acs.org/doi/10.1021/acsami.6b05261
- [4] X. Sheng, S. Wang, L. Yin, Flexible, stretchable, and biodegradable thin-film silicon photovoltaics, in: Advances in Silicon Solar Cells, Springer International Publishing, 2018, pp. 161–175. doi:10.1007/978-3-31969703-1<sub>6</sub>.http://link.springer.com/10.1007/978-3-319-69703-1<sub>6</sub>M.Nomura,J. Shiomi,T. Shi
- [6]5 M. Nomura, R. Anufriev, Z. Zhang, J. Maire, Y. Guo, R. Yanagisawa, S. Volz, Review of thermal transport in phononic crystals, Materials Today Physics 22 (2022) 100613. doi:10.1016/j.mtphys.2022.100613. URL https://linkinghub.elsevier.com/retrieve/pii/S2542529322000116
- [7] A. George, R. Yanagisawa, R. Anufriev, J. He, N. Yoshie, N. Tsujii, Q. Guo, T. Mori, S. Volz, M. Nomura, Thermoelectric enhancement of silicon membranes by ultrathin amorphous films, ACS applied materials & interfaces 11 (12) (2019) 12027–12031.
- [8] P. E. Hopkins, C. M. Reinke, M. F. Su, R. H. Olsson, E. A. Shaner, Z. C. Leseman, J. R. Serrano, L. M. Phinney, I. El-Kady, Reduction in the Thermal Conductivity of Single Crystalline Silicon by Phononic Crystal Patterning, Nano Letters 11 (1) (2011) 107–112. doi:10.1021/nl102918q. URL https://pubs.acs.org/doi/10.1021/nl102918q
- [9] J.-K. Yu, S. Mitrovic, D. Tham, J. Varghese, J. R. Heath, Reduction of thermal conductivity in phononic nanomesh structures, Nature Nanotechnology 5 (10) (2010) 718–721. doi:10.1038/nnano.2010.149.

- URL http://www.nature.com/articles/nnano.2010.149
- [10] J. Tang, H.-T. Wang, D. H. Lee, M. Fardy, Z. Huo, T. P. Russell, P. Yang, Holey Silicon as an Efficient Thermoelectric Material, Nano Letters 10 (10) (2010) 4279–4283. doi:10.1021/nl102931z.
  URL https://pubs.acs.org/doi/10.1021/nl102931z
- [11] J. Lim, H.-t. Wang, J. Tang, S. C. Andrews, H. So, J. Lee, D. H. Lee, T. P. Russell, P. Yang, Simultaneous Thermoelectric Property Measurement and Incoherent Phonon Transport in Holey Silicon, ACS Nano 10 (1) (2016) 124–132. doi:10.1021/acsnano.5b05385.
  URL https://pubs.acs.org/doi/10.1021/acsnano.5b05385
- [12] N. Liu, T. Zhu, M. Rosul, J. Peters, J. Bowers, M. Zebarjadi, Thermoelectric properties of holey silicon at elevated temperatures, Materials Today Physics 14 (2020) 100224. doi:10.1016/j.mtphys.2020.100224. URL https://linkinghub.elsevier.com/retrieve/pii/S2542529320300481
- [13] M. Nomura, Y. Kage, D. Müller, D. Moser, O. Paul, Electrical and thermal properties of polycrystalline Si thin films with phononic crystal nanopatterning for thermoelectric applications, Applied Physics Letters 106 (22) (2015) 223106. doi:10.1063/1.4922198. URL http://aip.scitation.org/doi/10.1063/1.4922198
- [14] T. Zhu, D. H. Olson, P. E. Hopkins, M. Zebarjadi, Heat diffusion imaging: Inplane thermal conductivity measurement of thin films in a broad temperature range, Review of Scientific Instruments 91 (11) (2020) 113701. doi:10.1063/5.0024476. URL http://aip.scitation.org/doi/10.1063/5.0024476
- [15] A. Stranz, J. Kähler, A. Waag, E. Peiner, Thermoelectric Properties of HighDoped Silicon from Room Temperature to 900 K, Journal of Electronic Materials 42 (7) (2013) 2381–2387. doi:10.1007/s11664-013-2508-0. URL http://link.springer.com/10.1007/s11664-013-2508-0
- [16] J. Ristein, Surface Transfer Doping of Semiconductors, Science 313 (5790) (2006) 1057–1058. doi:10.1126/science.1127589.

- URL https://www.science.org/doi/10.1126/science.1127589
- [17] L. Pfeiffer, K. W. West, H. L. Stormer, K. W. Baldwin, Electron mobilities exceeding 10<sup>7</sup> cm<sup>2</sup>/Vs in modulation-doped GaAs, Applied Physics Letters 55 (18) (1989) 1888–1890. doi:10.1063/1.102162. URL http://aip.scitation.org/doi/10.1063/1.102162
- [18] W. Gao, A. Kahn, Electronic structure and current injection in zinc phthalocyanine doped with tetrafluorotetracyanoquinodimethane: Interface versus bulk effects, Organic Electronics 3 (2) (2002) 53–63. doi:10.1016/S15661199(02)00033-2. URL https://linkinghub.elsevier.com/retrieve/pii/S1566119902000332
- [19] M. Pfeiffer, K. Leo, X. Zhou, J. Huang, M. Hofmann, A. Werner, J. Blochwitz-Nimoth, Doped organic semiconductors: Physics and application in light emitting diodes, Organic Electronics 4 (2-3) (2003) 89–103. doi:10.1016/j.orgel.2003.08.004.
  URL https://linkinghub.elsevier.com/retrieve/pii/S1566119903000235
- [20] J. Hynynen, D. Kiefer, C. Müller, Influence of crystallinity on the thermoelectric power factor of P3HT vapour-doped with F4TCNQ, RSC Advances 8 (3) (2018) 1593–1599. doi:10.1039/C7RA11912G. URL https://pubs.rsc.org/en/content/articlelanding/2018/ra/c7ra11912g
- [21] W. Chen, S. Chen, D. C. Qi, X. Y. Gao, A. T. S. Wee, Surface Transfer p-Type Doping of Epitaxial Graphene, Journal of the American Chemical Society 129 (34) (2007) 10418–10422. doi:10.1021/ja071658g. URL http://pubs.acs.org/doi/abs/10.1021/ja071658g
- [22] H. Pinto, R. Jones, J. P. Goss, P. R. Briddon, p-type doping of graphene with F4-TCNQ, Journal of Physics: Condensed Matter 21 (40) (2009) 402001. doi:10.1088/0953-8984/21/40/402001.
   URL https://iopscience.iop.org/article/10.1088/0953-8984/21/40/402001
- [23] R. Schlesinger, Y. Xu, O. T. Hofmann, S. Winkler, J. Frisch, J. Niederhausen, A. Vollmer, S. Blumstengel, F. Henneberger, P. Rinke, M. Scheffler, N. Koch, Controlling the work function of ZnO and the energylevel alignment at the interface to organic semiconductors with a molecular electron acceptor, Physical Review B 87 (15) (2013) 155311. doi:10.1103/PhysRevB.87.155311.

- URL https://link.aps.org/doi/10.1103/PhysRevB.87.155311
- [24] X. Wang, K. Esfarjani, M. Zebarjadi, First-Principles Calculation of Charge Transfer at the Silicon-Organic Interface, The Journal of Physical Chemistry C 121 (29) (2017) 15529–15537. doi:10.1021/acs.jpcc.7b03275. URL https://pubs.acs.org/doi/10.1021/acs.jpcc.7b03275
- [25] N. Liu, J. Peters, A. Ramu, J. A. Floro, J. E. Bowers, M. Zebarjadi, Thermoelectric transport at F 4 TCNQ-silicon interface, APL Materials 7 (2) (2019) 021104. doi:10.1063/1.5050537. URL http://aip.scitation.org/doi/10.1063/1.5050537
- [26] H. Ohta, S. Kim, Y. Mune, T. Mizoguchi, K. Nomura, S. Ohta, T. Nomura, Y. Nakanishi, Y. Ikuhara, M. Hirano, H. Hosono, K. Koumoto, Giant thermoelectric seebeck coefficient of a two-dimensional electron gas in srtio₃, Nature Materials 6 (2) (2007) 129–134. doi:10.1038/nmat1821. URL https://www.nature.com/articles/nmat1821
- [27] M. Zebarjadi, G. Joshi, G. Zhu, B. Yu, A. Minnich, Y. Lan, X. Wang, M. Dresselhaus, Z. Ren, G. Chen, Power Factor Enhancement by Modulation Doping in Bulk Nanocomposites, Nano Letters 11 (6) (2011) 2225–2230. doi:10.1021/nl201206d.
  URL https://pubs.acs.org/doi/10.1021/nl201206d
- [28] B. Yu, M. Zebarjadi, H. Wang, K. Lukas, H. Wang, D. Wang, C. Opeil, M. Dresselhaus, G. Chen, Z. Ren, Enhancement of Thermoelectric Properties by Modulation-Doping in Silicon Germanium Alloy Nanocomposites, Nano Letters 12 (4) (2012) 2077–2082. doi:10.1021/nl3003045. URL https://pubs.acs.org/doi/10.1021/nl3003045
- [29] J. Maire, E. Chávez-Ángel, G. Arregui, M. F. Colombano, N. E. Capuj, A. Griol, A. Martínez, D. Navarro-Urrios, J. Ahopelto, C. M. Sotomayor-Torres, Thermal Properties of Nanocrystalline Silicon Nanobeams, Advanced Functional Materials 32 (4) (2022) 2105767. doi:10.1002/adfm.202105767. URL https://onlinelibrary.wiley.com/doi/10.1002/adfm.202105767
- [30] K. Valalaki, N. Vouroutzis, A. G. Nassiopoulou, Significant enhancement of the thermoelectric figure of merit of polycrystalline Si films by reducing

- grain size, Journal of Physics D: Applied Physics 49 (31) (2016) 315104. doi:10.1088/0022-3727/49/31/315104. URL https://iopscience.iop.org/article/10.1088/0022-3727/49/31/315104
- [31] M. A. Leitch-Devlin, D. A. Williams, Sticking coefficients for atoms and molecules at the surfaces of interstellar dust grains, Monthly Notices of the Royal Astronomical Society 213 (2) (1985) 295–306. doi:10.1093/mnras/213.2.295. URL https://academic.oup.com/mnras/article-lookup/doi/10.1093/mnras/213.2.295
- [32] M. Levinshtein, S. Rumyantsev, M. Shur (Eds.), Handbook Series on Semiconductor Parameters, World Scientific Publishing Co. Pte. Ltd., 1996. doi:10.1142/9789812832078. URL http://ebooks.worldscinet.com/ISBN/9789812832078/9789812832078.html
- [33] W. Gao, A. Kahn, Controlled p-doping of zinc phthalocyanine by coevaporation with tetrafluorotetracyanoquinodimethane: A direct and inverse photoemission study, Applied Physics Letters 79 (24) (2001) 4040– 4042. doi:10.1063/1.1424067. URL http://aip.scitation.org/doi/10.1063/1.1424067
- [34] J. A. Dillon, H. E. Farnsworth, Work Function and Sorption Properties of Silicon Crystals, Journal of Applied Physics 29 (8) (1958) 1195–1202. doi:10.1063/1.1723401. URL http://aip.scitation.org/doi/10.1063/1.1723401
- [35] V. Kessler, D. Gautam, T. Hülser, M. Spree, R. Theissmann, M. Winterer, H. Wiggers, G. Schierning, R. Schmechel, Thermoelectric Properties of Nanocrystalline Silicon from a Scaled-Up Synthesis Plant, Advanced Engineering Materials 15 (5) (2013) 379–385. doi:10.1002/adem.201200233. URL https://onlinelibrary.wiley.com/doi/10.1002/adem.201200233
- [36] Y. Ohishi, J. Xie, Y. Miyazaki, Y. Aikebaier, H. Muta, K. Kurosaki, S. Yamanaka, N. Uchida, T. Tada, Thermoelectric properties of heavily boron- and phosphorus-doped silicon, Japanese Journal of Applied Physics 54 (7) (2015) 071301. doi:10.7567/JJAP.54.071301.
  URL https://iopscience.iop.org/article/10.7567/JJAP.54.071301